Voltage Unbalance Mitigation in Low Voltage Distribution Networks using Time Series Three-Phase Optimal Power Flow

Mohammad A.A. Al-Ja'afreh, Geev Mokryani

Faculty of Engineering and Informatics, University of Bradford, BD7 1DP, UK
m.a.a.al-jaafreh@bradford.ac.uk; g.mokryani@bradford.ac.uk

Abstract— **Due to high penetration of single-phase Photovoltaic (PV) cells into low voltage (LV) distribution networks, several impacts such as voltage unbalance, voltage rise, power losses, reverse power flow arise which leads to operational constraints violation in the network. In this paper, a time series Three Phase Optimal Power Flow (TPOPF) method is proposed to minimize the voltage unbalance in LV distribution networks with high penetration of residential PVs. TPOPF problem is formulated using the current injection method in which the PVs are modelled via a time-varying PV power profile with active and reactive power control. The proposed method is validated on a real LV distribution feeder. The results show that the reactive power management of the PVs helps mitigate the voltage unbalance significantly. Moreover, the voltage unbalance index reduced significantly compared to the case without voltage unbalance minimisation.**

Index Terms: **Low voltage distribution networks, current injection method, voltage unbalanced, three-phase optimal power flow.**

NOMENCLATURE

$V_{r,i,Neg}, V_{Im,i,Neg}$	Real and imaginary parts of the negative sequence voltage $V_{i,Neg}$ at bus i
Ω_u , Ω_k	Set of buses where the voltage unbalance is to be minimized, and set of buses directly connected to the bus k respectively
T	Set of time series.
V_i^a, V_i^b, V_i^c	Three-phase voltages at bus i
$P_{control-pv}$	Active PV power control variable
$\mathrm{Tan}\,\Phi_{control-pv}$	Reactive PV power control variable
$V_{i,Pos}, V_{i,Neg}$	Positive and negative sequence voltage components at bus i
ΔI_K^s	Three-phase current mismatches for a given bus.
$(P_k^{sp})^s, (Q_k^{sp})^s$	Active and reactive powers at the bus k for a given phase s
G_{ki}^{st}, B_{ki}^{st}	Nodal admittance matrix components
$(E_k^s)^*$	The complex conjugate voltage at bus k
P_{Gk}^s, Q_{Gk}^s	Active and reactive powers generated for a given phase s
P_{Lk}^s, Q_{Lk}^s	Active and reactive powers of loads for a given phase s
$P_{zk}^s, P_{Ik}^s, P_{Pk}^s$	ZIP component of active power load demand at bus k and phases s
$Q_{zk}^s, Q_{Ik}^s, Q_{Pk}^s$	ZIP component of reactive power load demand at bus k and phases s
$P_{pv}{}^s$, $Q_{pv}{}^s$	The injected active and reactive power for each PV
$P_{sp}{}^{pv}$	The value of the PV Power profile
V_k^s	Steady-state voltage magnitude at bus k and phase s
$V_{\max k}^s, V_{\min k}^s$	The maximum and minimum voltage limits for bus k and phase s
I_l^s	The current flowing through each phase s of each line l
$I_{l\max}^s$	Rated cable current
S_{Trans}^s	Total apparent power flow through the substation transformer
$S_{Trans\_rating}^s$	substation transformer rating power

I. INTRODUCTION

A. Motivation and Background

There has been a considerable increase in photovoltaic (PV) penetration in low voltage (LV) distribution networks in recent years. Despite the numerous advantages of the grid-connected PVs systems, the high penetration of PVs into distribution networks could lead to several negative impacts such as reverse power flow, voltage increase, power losses, voltage unbalance and an increase of reactive power [1]. Besides the effects on voltage unbalances, solar radiation has a direct impact on PV system production, which can introduce a dynamical (time-varying) aspect to the problem. The voltage unbalances in LV distribution networks can be costly and produce undesirable operational conditions [2]. Technologies are now available for the economic implementation of introducing voltage control. For instance, active network management (ANM) schemes have the capability to mitigate undesirable operational conditions in PV-rich LV distribution networks [3].

B. Literature Review and Research Gap

Previous research works [5-10] have proposed power flow techniques which considered the voltage unbalance in LV distribution networks which cover a wide range of the operational challenges in LV networks posed by the adoption of Low Carbon Technologies (LCTs).

The three-phase current injection method (TPCIM) has proven its capability as an efficient power flow method for radial and meshed distribution networks. It was initially developed by [4] and later used by various researchers to formulate a variety of developed techniques. Reference [5-7] focused on power flow techniques taking only snapshot approaches (static demand and static load model) into consideration. [8-10] have taken into account realistic operating considerations such as the time-varying nature of load demand. However, the corresponding voltage dependent load models, critical to quantify demand reduction, have been primarily neglected in previous works.

Previous works [8-10] do not consider detailed network (three-phase) and load modelling to define the LV customers in a more realistic model.

From an operational perspective, the majority of these studies limit their time resolution to one hour while the load demand and the generation can change significantly in minute scale. Furthermore, the system state variables (e.g., the voltage at each bus)should consider the minute scale variations rather than hourly ones, thus, ignoring minute-scale changes in demand and generation results in voltage violations. Consequently, more realistic, and granulated network and load models are required to adequately quantify opportunities for voltage unbalance minimization and the associated operational aspects. Table 1 summarizes a taxonomy of proposed method.

TABLE 1 COMPARING PROPOSED METHOD WITH EXISTING METHODS

Reference	Network type/Topology	Time series/ resolution	PV power control	Voltage dependence load model
[5]	DN*(Radial)	No	Yes (Reactive)	No
[6]	DN(Radial)	No	Yes (Reactive)	Yes
[7]	DN(Radial)	No	No	No
[8]	DN(Radial)	Yes (1 hr)	Yes (Reactive)	No
[9]	DN(Radial)	Yes (1 hr)	No	No
[10]	DN(Radial)	Yes (1 hr)	No	No
Proposed method	**DN (Radial and Meshed)**	**Yes (10 min)**	**Yes (Active and reactive)**	**Yes**

DN*: Distribution network

C. Contributions

In this paper, a Time series Three-Phase Optimal Power Flow method (TPOPF) is proposed to minimize the voltage unbalance in LV distribution networks with high penetration of residential PVs. The time series TPOPF method used for the integration of grid-connected PVs with the capability of controlling both active and reactive power injection to the system. The main contributions of this paper are as follows:

1. Propose a time series TPOPF method with 10 min time resolution to mitigate the voltage unbalance in PV-rich LV distribution networks.
2. Model and formulate the LV network components using a detailed and accurate model (e.g., all house load demand modelled as time-variant and voltage-dependent models (ZIP modelling)). Also, an integrated model of the grid-connected PVs with the capability of controlling both active and reactive power injection to the network has been tested. The PV reactive power control is accomplished using voltage regulation of the PV inverter to maintain the voltage within acceptable limits when they operate during peak solar irradiation.

II. METHODOLOGY

Three simulation platforms have been used to model and simulate the Proposed TPOPF method as follows: (a) OpenDSS platform [11], (b) Python, has been interfaced with OpenDSS through a COM interface [11], and (c) Pyomo library under python simulation platform, has been used to create the optimization problem model [12]. Furthermore, nonlinear optimization solver KNITRO has been used to solve the nonlinear optimization problem [13].

III. PROBLEM FORMULATION

This section defines the key expressions that comprise the TPOPF formulation.

A. Objective function

The objective of the OPF problem, equation (1), is to minimize the total voltage unbalance in the network. To attain this objective, the objective function is formulated to minimize the sum of the absolute values of the negative sequence system voltages.

$$\min \sum_{i \in \Omega u} \sum_{t \in T} \left(V_{r,i,Neg}^2 + V_{Im,i,Neg}^2 \right) \tag{1}$$

$$V_{i,Neg} = V_i^a + \alpha^2 V_i^b + \alpha V_i^c \text{ and } \alpha = 1 \prec 120° \tag{2}$$

The unbalance index (UI) is used to assess the unbalance condition on each bus [14]. The overall system unbalance conditions are determined by computing the summation of the square of individual UIs, as described in equations (3-4):

$$UI_{system} = \left(\sum_{i \in \Omega_k} \sum_{t \in T} \frac{\left| V_{i,Neg}^2 \right|}{\left| V_{i,Pos}^2 \right|} \right) \times 100\% \tag{3}$$

$$V_{i,Pos} = V_i^a + \alpha \, V_i^b + \alpha^2 V_i^c \tag{4}$$

B. Defining the nodal current injection

For a given bus k and phase s the three-phase current mismatches are formulated in (5-10):

$$\Delta I_K^s = \frac{(P_k^{sp})^s - j(Q_k^{sp})^s}{(E_k^s)^*} - \sum_{i \in \Omega_k} \sum_{t \in \alpha_p} Y_{ki}^{st} E_i^t \tag{5}$$

where $S, t \in \alpha_p$, $\alpha_p = \{a, b, c\}$, $k = \{1, ..., n\}$, n is the total number of buses

$$E_k = V_{rk} + jV_{imk} \tag{6}$$

$$(P_k^{sp})^s = P_{Gk}^s - P_{Lk}^s \tag{7}$$

$$(Q_k^{sp})^s = Q_{Gk}^s - Q_{Lk}^s \tag{8}$$

The voltage level's effect on the power of the system loads is modelled as follows:

$$P_{Lk}^s = P_{zk}^s \left(\frac{V_k^s}{V_k^{nom}} \right)^2 + P_{Ik}^s \left(\frac{V_k^s}{V_k^{nom}} \right) + P_{Pk}^s \tag{9}$$

$$Q_{Lk}^s = Q_{zk}^s \left(\frac{V_k^s}{V_k^{nom}} \right)^2 + Q_{Ik}^s \left(\frac{V_k^s}{V_k^{nom}} \right) + Q_{Pk}^s \tag{10}$$

Equations (11-12) define the specified active $(P_k^{sp})^s$ and reactive $(Q_k^{sp})^s$ power injections, respectively.

$$(P_k^{sp})^s = P_{Gk}^s - P_{zk}^s \left(\frac{V_k^s}{V_k^{nom}} \right)^2 + P_{Ik}^s \left(\frac{V_k^s}{V_k^{nom}} \right) + P_{Pk}^s \tag{11}$$

$$(Q_k^{sp})^s = Q_{Gk}^s - Q_{zk}^s \left(\frac{V_k^s}{V_k^{nom}} \right)^2 + Q_{Ik}^s \left(\frac{V_k^s}{V_k^{nom}} \right) + Q_{Pk}^s \tag{12}$$

Equation (6) is further presented in terms of its $\Re$ and $\Im$ parts as follows (13-14):

$$\Delta I_{rK}^s = \frac{(P_k^{sp})^s V_{rk}^s + j(Q_k^{sp})^s V_{Imk}^s}{(V_{rk}^s)^2 + (V_{Imk}^s)^2} - \sum_{i \in \Omega_k} \sum_{t \in \alpha_p} \left(G_{ki}^{st} V_{ri}^t - B_{ki}^{st} V_{Imi}^t \right) \tag{13}$$

$$\Delta I_{ImK}^s = \frac{(P_k^{sp})^s V_{Imk}^s - j(Q_k^{sp})^s V_{rk}^s}{(V_{rk}^s)^2 + (V_{Imk}^s)^2} - \sum_{i \in \Omega_k} \sum_{t \in \alpha_p} \left(G_{ki}^{st} V_{Imi}^t - B_{ki}^{st} V_{ri}^t \right) \tag{14}$$

Equations (14-15) are written in terms of the specified and calculated values as follows:

$$\Delta I^s_{rK} = (I^{sp}_{rK})^s - (I^{calc}_{rK})^s \tag{15}$$

$$\Delta I^s_{\text{Im}k} = (I^{sp}_{\text{Im}k})^s - (I^{calc}_{\text{Im}k})^s \tag{16}$$

The $\Re$ and $\Im$ calculated currents are expressed in (17-18).

$$(I^{Calc}_{rk})^s = \sum_{i\in\Omega_k}\sum_{t\in\alpha_p}\left(G^{st}_{ki}V^t_{ri} - B^{st}_{ki}V^t_{\text{Im}i}\right) \tag{17}$$

$$(I^{Calc}_{\text{Im}k})^s = \sum_{i\in\Omega_k}\sum_{t\in\alpha_p}\left(G^{st}_{ki}V^t_{\text{Im}i} + B^{st}_{ki}V^t_{ri}\right) \tag{18}$$

C. Lines and cable modelling

Resistances, inductances, and capacitances (RLC) are used to model three-phase lines, cables, and some components. Figure 1 Shows the RLC equivalent circuit[14].
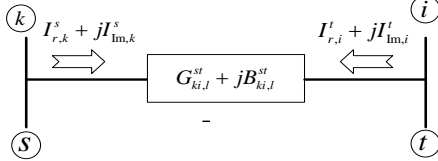
Figure 1. Model of cable, lines and RLC [14]

The elements $G^{st}_{ki,l}$ and $B^{st}_{ki,l}$ are real 3x3 matrices built from the component parameters. Each component is connected between nodes k and i as in Equation (19).

$$\begin{bmatrix} I^s_{\text{Im},k} \\ I^s_{r,k} \\ \vdots \\ I^s_{\text{Im},i} \\ I^s_{r,i} \end{bmatrix} = \begin{bmatrix} B^{st}_{ki,l} & G^{st}_{ki,l} & -B^{st}_{ki,l} & -G^{st}_{ki,l} \\ G^{st}_{ki,l} & -B^{st}_{ki,l} & -G^{st}_{ki,l} & B^{st}_{ki,l} \\ & \ddots & & \\ -B^{st}_{ki,l} & -G^{st}_{ki,l} & B^{st}_{ki,l} & G^{st}_{ki,l} \\ -G^{st}_{ki,l} & B^{abc} & G^{st}_{ki,l} & -B^{st}_{ki,l} \end{bmatrix} \cdot \begin{bmatrix} V^t_{r,k} \\ V^t_{\text{Im},k} \\ \vdots \\ V^t_{r,i} \\ V^t_{\text{Im},i} \end{bmatrix} \tag{19}$$

where $\begin{bmatrix} I^s_{\text{Im},k} & I^s_{\text{Re},k}\end{bmatrix}$ and $\begin{bmatrix} I^s_{\text{Im},i} & I^s_{r,i}\end{bmatrix}$ are real 6×1 vector expressing the real and imaginary parts of three-phase current injection into phase a, b and c of buses k and i. $\begin{bmatrix} V^t_{\text{Im},k} & V^t_{r,k}\end{bmatrix}$ and $\begin{bmatrix} V^t_{\text{Im},i} & V^t_{r,i}\end{bmatrix}$ are real 6×1 vector expressing the real and imaginary parts of nodal voltages into phase a, b and c of buses k and i.

The $\Re$ and $\Im$ current flow at each phase s of every line l are expressed in (21-22).

$$(I^{flow}_{rl})^s = \sum_{t\in\alpha_p}\left[G^{st}_{ki,l}(V^t_{ri} - V^t_{rk}) - B^{st}_{ki,l}(V^t_{\text{Im}i} - V^t_{\text{Im}k})\right] \tag{20}$$

$$(I^{flow}_{\text{Im}l})^s = \sum_{t\in\alpha_p}\left[G^{st}_{ki,l}(V^t_{\text{Im}i} - V^t_{\text{Im}k}) + B^{st}_{ki,l}(V^t_{ri} - V^t_{rk})\right] \tag{21}$$

D. Equality constraints

- **Current mismatch:** The current mismatches formulated in equations (16-17) are forced to be zero as in (22):

$$\Delta I^s = 0 \tag{22}$$

- **Slack bus:** The voltage on the slack bus, V^s_{slack}, must be equal to a specified value $\left(V^s_{sp}\right)_{slack}$ as defined in equation (23)

$$V^s_{slack} = \left(V^s_{sp}\right)_{slack} \tag{23}$$

E. Inequality constraints

Voltage limits, Current limits, and Transformer power limits are shown as follows :

$$V^s_{\min k} \leq V^s_k \leq V^s_{\max k} \tag{24}$$

$$I^s_l \leq I^s_{l\max} \tag{25}$$

$$\sum_{s\in\alpha_p} S^s_{Trans} \leq S^s_{Trans\_rating} \tag{26}$$

F. PV model

- **PV profiles**

PV profiles are chosen from a group of 100 profiles detailed in [15]. Given the restricted geographic extent of LV feeders, solar irradiance is presumed to be consistent across all consumers. Each house is presumed to have a PV (a worst-case voltage impacts scenario). The PV inverter considers a varying power factor (PF) with 0.95 leading and lagging boundaries. The $S^{pv}_{inverter}$ (PV inverter rating), is assumed to be 10 percent beyond the PV system power capacity.

- **PV active and reactive power inverter control**

PV inverters can absorb reactive power. This capability, associated with active power curtailment, is used to regulate the PV generation via the two controllable variables $P^{pv}_{control}$ and $\text{Tan}\,\Phi^{pv}_{control}$ as described in equations (27-31) [16].

$$P^s_{pv} = P^s_{pv,sp} P^{pv}_{control} \tag{27}$$

$$0 \leq P^{pv}_{control} \leq 1 \tag{28}$$

$$Q^s_{pv} = P^s_{pv}\,\text{Tan}\,\Phi^{pv}_{control} \tag{29}$$

$$-\tan(a\cos(\Phi)) \leq \text{Tan}\,\Phi^{pv}_{control} \leq \tan(a\cos(\Phi)) \tag{30}$$

$$\sqrt{(P^{pv})^2 + (Q^{pv})^2} \leq S^{pv}_{inverter} \tag{31}$$

$$Q^s_{pv}\min = -P^s_{pv}\times\tan(a\cos(\Phi)) \qquad Q^s_{pv}\max = P^s_{pv}\times\tan(a\cos(\Phi))$$
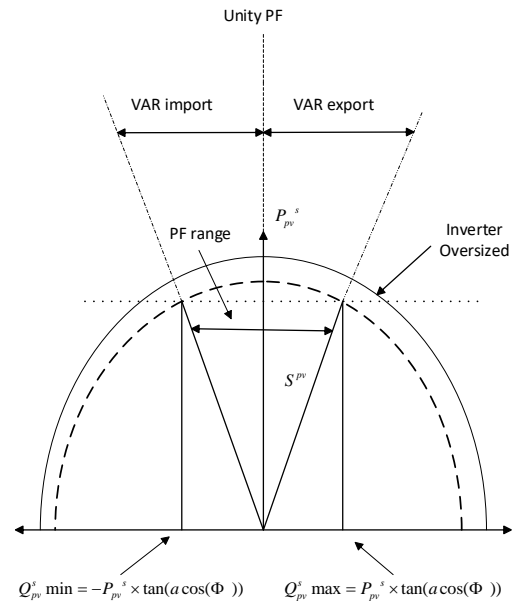
Figure 2 . PV inverter capability curve

Figure 2 illustrates the capability curve of a photovoltaic inverter. The active and reactive power is represented by the

y- and x-axes, respectively. The inverter power limit is indicated by the dashed line. As the inverter is limited by the PV active power rating, it cannot operate beyond this curve. It should be noted that the injected power is limited by the ratting of the PV inverter, making it impossible to operate at maximum active and reactive power at the same time. The dotted lines represent the PVs' active power injection limit due to the power factor, which is 0.95 in this case. Within the prescribed limits, the inverter will supply reactive power, which is, $Q_{P_V}^s \min$ and $Q_{P_V}^s \max$.

G. Angular Reference

The voltages on the system slack bus are usually balanced. As a result, additional equations are needed to ensure that the voltage phase shift is 120 degrees, as illustrated in Equation (32).

$$V_{\operatorname{Im} k}^a - V_{rk}^a \tan\left(\frac{0\pi}{180}\right) = 0$$
$$V_{\operatorname{Im} k}^b - V_{rk}^b \tan\left(\frac{-120\pi}{180}\right) = 0 \qquad (32)$$
$$V_{\operatorname{Im} k}^c - V_{rk}^c \tan\left(\frac{+120\pi}{180}\right) = 0$$

The above-described nonlinear optimization problem solved using the interior point technique due to its features such as fast convergence and efficient handling of inequality constraints.

IV. CASE STUDY

The proposed method is validated on a real LV distribution network in the United Kingdom (UK). The network is comprised of 83 houses (domestic load) with installed small-scale PVs. A detailed description of the network data provided in [16].

A. The model of the Network

The investigated network is based on a real network provided by Electricity North West Limited (ENWL) in the UK [15]. It serves 83 single-phase residential customers across one radial feeder, as shown in Figure 3. The nominal voltage of the LV network is 0.4 kV, while the nominal voltage of the medium voltage network is 10 kV. According to the EN 50160 standard [17], the upper and lower voltage statutory limits of +10% and −6%, is applied [17]. The distribution transformer has an 800 kVA rating.
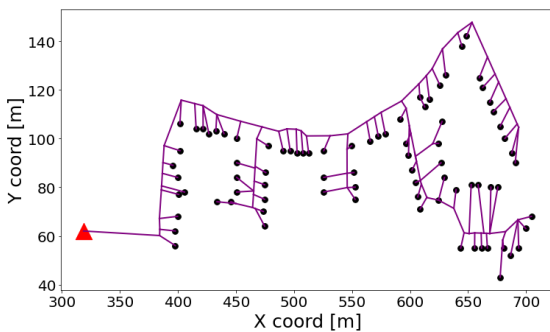

Figure 3. ENWL simplified network model. The houses represented by black dots. The distribution substation represented by the red triangle

B. Residential customers Profiles

The model from [18] is used to generate a group of 100 domestic load profiles. This model generates daily time-series profiles for residential loads that consider occupancy of the house, thermal operation, activities, and electrical appliances. The generated profiles have a 10-minute resolution and describe the active or reactive power load demand in terms of the ZIP load model, constant impedance (Z), constant current (I) and constant power (P).

V. SIMULATION RESULT AND DISCUSSIONS

The system under study is simulated twice with and without voltage unbalance minimization. The objective function for the Three Phase Optimal Power Flow (TPOPF) is minimizing the voltage unbalanced in the LV network. The PV penetration is 80% (i.e., 80% of houses in the system have a single-phase rooftop PV system). The solution of the TPOPF is resulting in active and reactive power injection from the PV at each bus characteristic by the controllable variables ($P_{control}^{Pv}$ and $Tan\ \varphi_{control}^{Pv}$) and the power injected from the substation subjected to the system constraint.

Figure 4 shows the voltage magnitude across all nodes at all buses (three phases for each bus) of the system. It can be observed that the voltage has not exceeded the upper/lower limits (+10%, -6%). Figure 5 shows the voltage at the end of the feeder. The voltage at the end of the feeder can be used as an indicator of the voltage drop across the system. It can be observed that the voltage on the last bus of the system is within the limit. Moreover, the dotted lines refer to the results without voltage unbalance minimisation and the solid lines indicate the voltage at the selected bus minimising the voltage unbalance. The voltage displacement among the three phases reduced between 40%-80% approximately at all buses at hours 5:00-18:00.

Figure 6 shows the individual UI at all load buses for both the cases with (solid line) and without (dotted line) voltage unbalance minimisation. The overall system UI without voltage unbalance minimization is 29.4×10⁻³ and the with voltage unbalance minimization is 8.9 ×10⁻³. It is evident that the UI % reduced by 69 % at all load buses. Also, Figure 6 shows that the UI without unbalance minimization (dotted line) goes beyond 2 % at different buses (e.g., feeder2-48, feeder2-611). Figure 7 shows the relationship between the voltage unbalance index (UI) at a specific bus and the derating factor of any machine connected to this bus. As can be seen in Figure 8, the derating factor of a machine is inversely proportional to the bus UI. Moreover, Reference [14] conclude that the derating factor of the equipment (electric machine) connected to a load bus with UI above 1% decrease exponentially which resulted in reducing the useful life of the machine as illustrated in Figure 6. For example, if a machine connected to bus *feeder2-48* with an approximate UI of 3 %, this could lead to a possible derating factor of the machine (0.89) as shown in Figure 7. This exemplifies the type of issue that can be resolved. using the proposed time series TPOPF.
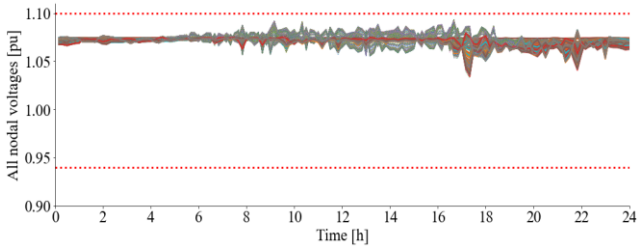
Figure 4. Voltage magnitude across all nodes at all buses in the system
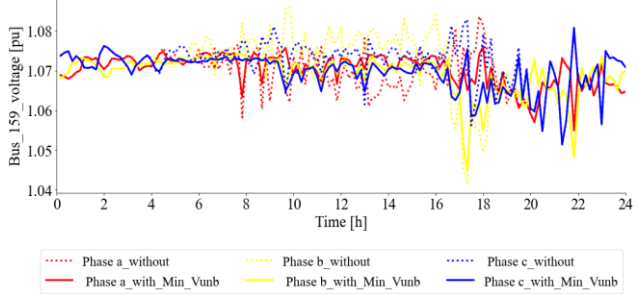

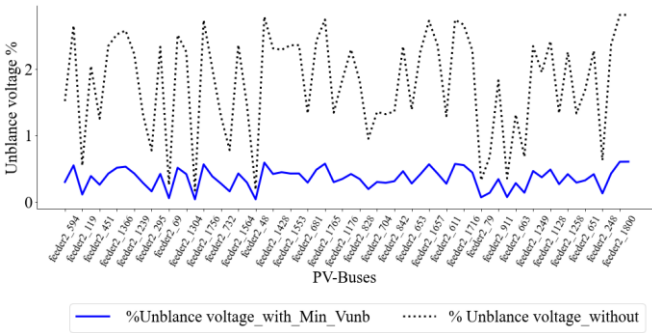Figure 5. The voltage at the end of the feeder

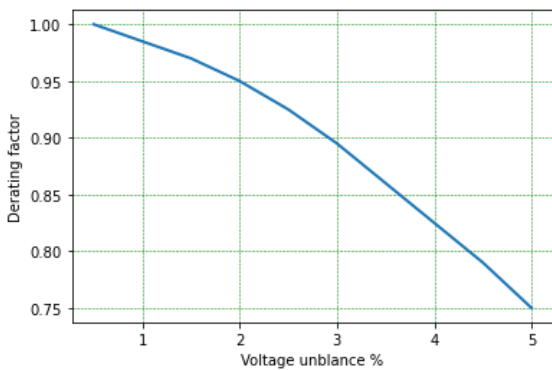Figure 6. Voltage Unbalance index at the PV buses

Figure 7. Machine derating factor [14].

Figure 8 shows the total load demand at all phases of the system for time step T (at each hour). Figure 9 shows the total real power generated by the PVs at each time step T, and Figure 8 shows the total real power supplied from the substation at each time step T. From Figures 8-10, it can be observed that the load demand is supplied from the substation when the PV is not generating or not capable to meet the total load demand. For example, the PV system is not generating at the night-time period (T= 0-4h and 20-24h), so in this case, the total load demand is supplied from the substation as shown in Figure 10. If the PV is not generating enough electricity to meet the load demand, the rest of the power is supplied from the substation. For

example, at T=18 in phase b, the total load demand is around 35 kW, however, the PV is only generating 10 kW. So, the rest of the power is supplied from the substation, which is about 25 kW.

Figure 11 and Figure 12 show the values of the controllable variables $P_{control}^{Pv}$ and $Tan\,\varphi_{control}^{Pv}$. These variables represent the inverter's operation at each PV system. $P_{control}^{Pv}$ limits the level of active power injected into the networks by each PV and $Tan\,\varphi_{control}^{Pv}$ limits the reactive power injected or absorbed by each PV. The results are shown in terms of median, 1st and 99th percentile. A percentile is a measure in statistics. It shows the value below which a given percentage of observations falls. For example, the 99th percentile is the value (or score) below which 99% of the observations may be found. In other words, if the value falls in the top 1 %, so it is in the 99th percentile.

It is observed from Figure 11 and Figure 12 that the reactive power consumption and the active power curtailment occur at each time step for each PV to comply with the constraints (Equation 22-26) and to minimize the total system voltage unbalanced. Furthermore, the control variable $Tan\,\varphi_{control}^{Pv}$ is controlling the reactive power consumption to keep the system voltage within the statutory limit. The active power curtailment happens at different periods to minimize the total system voltage unbalanced.

In other words, the system tends to reduce the power injection into the buses by curtailed the PVs active power at different periods (e.g., T=6,8,10 and 12). It is worth mentioning that the PV operation at each period significantly depends on its location. The PV at the end of the feeder (i.e., which has a high impedance path to the substation) will tend to work at lower PF and higher curtailment to reduce their impact on the feeder voltages.
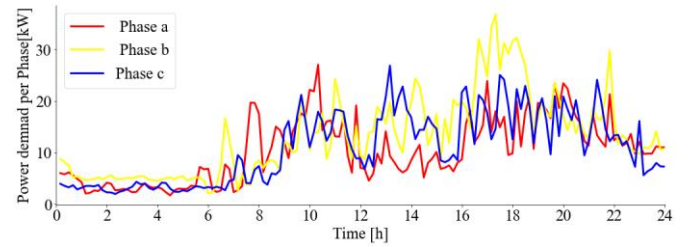

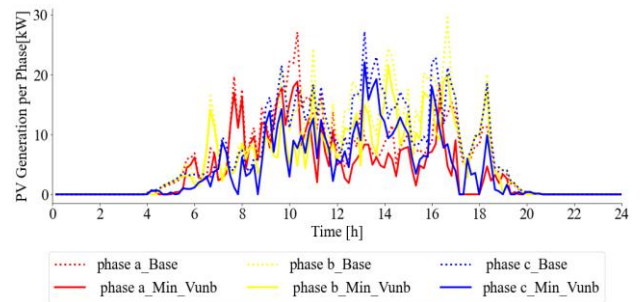Figure 8. The total load demand at each phase of the feeder

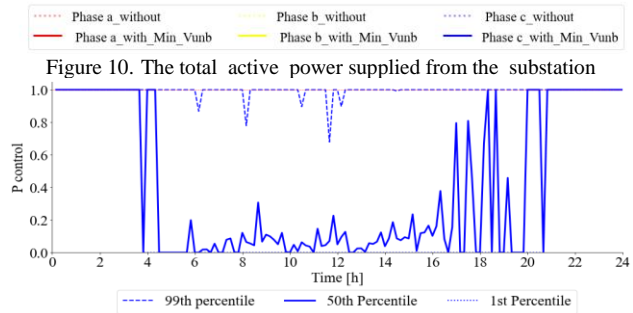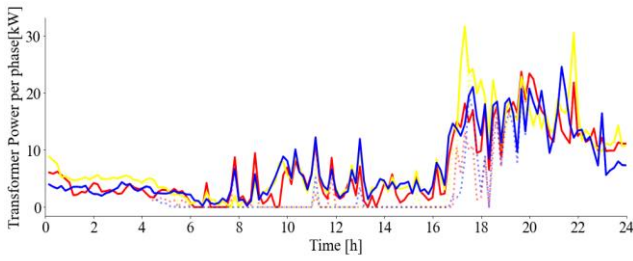Figure 9. The total active power generation from the PV

Figure 10. The total active power supplied from the substation

Figure 11. The value of the Variable P-Control at minimizing the total voltage unbalance
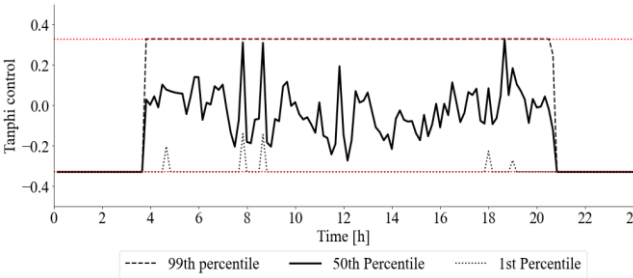

Figure 12 The value of the variable Tan-Phi -control at minimizing the total voltage unbalance

VI. CONCLUSION

In this paper, a time series TPOPF method to minimize the voltage unbalance in the PV-rich LV distribution network is proposed. The optimization problem was formulated using the current injection method. The PVs output power are modelled via a time-varying PV power profile with an active power control variable. Reactive PV power control achieved through the application of the voltage regulation function of the inverter, which can operate as a reactive power compensator. The effectiveness of the proposed method verified using a case study of a real LV distribution feeder and simulated with and without voltage unbalance minimisation. The results show that the reactive power management of the PVs can mitigate the voltage unbalance significantly. Moreover, the voltage unbalance index reduced by 69% using the proposed method.

ACKNOWLEDGEMENT

REFERENCES

[1] K. A. Alboaouh and S. Mohagheghi, "Impact of Rooftop Photovoltaics on the Distribution System," *J. Renew. Energy*, vol. 2020, pp. 1–23, 2020, doi: 10.1155/2020/4831434.

[2] G. P. Systems and M. E. Ayikpa, "An Efficient Tool for Mitigating Voltage Unbalance with Reactive Power Control of Distributed," vol. 11, no. 2, pp. 187–195, 2017.

[3] L. Gutierrez-Lagos and L. F. Ochoa, "OPF-Based CVR Operation in PV-Rich MV-LV Distribution Networks," *IEEE Trans. Power Syst.*, vol. 34, no. 4, pp. 2778–2789, 2019, doi: 10.1109/TPWRS.2019.2894795.

[4] P. A. N. Garcia *et al.*, "Three-Phase Power Flow Calculations Using the Current Injection Method," vol. 15, no. 2, pp. 508–514, 2000.

[5] R. Anilkumar, G. Devriese, and A. K. Srivastava, "Voltage and Reactive Power Control to Maximize the Energy Savings in Power Distribution System with Wind Energy," *IEEE Trans. Ind. Appl.*, vol. 54, no. 1, pp. 656–664, 2018, doi: 10.1109/TIA.2017.2740850.

[6] G. Mokryani, A. Majumdar, and B. C. Pal, "Probabilistic method for the operation of three-phase unbalanced active distribution networks," *IET Renew. Power Gener.*, vol. 10, no. 7, pp. 944–954, 2016, doi: 10.1049/iet-rpg.2015.0334.

[7] G. Mokryani and P. Siano, "Strategic placement of distribution network operator owned wind turbines by using market-based optimal power flow," *IET Gener. Transm. Distrib.*, vol. 8, no. 2, pp. 281–289, 2014, doi: 10.1049/iet-gtd.2013.0288.

[8] A. Padilha-Feltrin, D. A. Quijano Rodezno, and J. R. S. Mantovani, "Volt-VAR Multiobjective Optimization to Peak-Load Relief and Energy Efficiency in Distribution Networks," *IEEE Trans. Power Deliv.*, vol. 30, no. 2, pp. 618–626, 2015, doi: 10.1109/TPWRD.2014.2336598.

[9] A. Selim, M. Abdel-Akher, M. M. Aly, and S. Kamel, "Efficient time series simulation of distribution systems with voltage regulation and PV penetration," *2016 18th Int. Middle-East Power Syst. Conf. MEPCON 2016 - Proc.*, pp. 717–722, 2017, doi: 10.1109/MEPCON.2016.7836972.

[10] G. Mokryani and P. Siano, "Optimal wind turbines placement within a distribution market environment," *Appl. Soft Comput. J.*, vol. 13, no. 10, pp. 4038–4046, 2013, doi: 10.1016/j.asoc.2013.05.019.

[11] "OpenDSS." Electric Power Reserch Institute EPRI, USA, [Online]. Available: https://smartgrid.epri.com/SimulationTool.aspx.

[12] and D. L. W. Hart, William E., Jean-Paul Watson, "Pyomo: modeling and solving mathematical programs in Python." Mathematical Programming Computation, 2020, [Online]. Available: http://www.pyomo.org/.

[13] "Knitro." artelys, 2020, [Online]. Available: https://www.artelys.com/solvers/knitro

[14] L. R. Araujo, D. R. R. Penido, S. Member, S. Carneiro, J. L. R. Pereira, and S. Member, "A Three-Phase Optimal Power-Flow Algorithm to Mitigate Voltage Unbalance," vol. 28, no. 4, pp. 2394–2402, 2013.

[15] ENWL, "Low Voltage Network Solutions (LVNS)," 2014. https://www.enwl.co.uk/zero-carbon/innovation/smaller-projects/low-carbon-networks-fund/low-voltage-network-solutions/.

[16] V. Rigoni and A. Keane, "Open-DSOPF : an open-source optimal power flow formulation integrated with OpenDSS," no. April, 2020.

[17] H. Markiewicz and A. Klajn, "Voltage Disturbances Standard EN 50160 Voltage Characteristics in Public Distribution Systems"

[18] K. Mckenna, S. Member, A. Keane, and S. Member, "Residential Load Modeling of Price Based Demand Response for Network Impact Studies," 2015